First-principles study of hydrogen ordering in lanthanum hydride and its effect on the metal-insulator transition

Tobias C. Kerscher,[1,2,*] Gunther Schöllhammer,[2] Peter Herzig,[2] Walter Wolf,[3] Raimund Podloucky,[2] and Stefan Müller[1]

[1]*Hamburg University of Technology, Institute of Advanced Ceramics, Denickestraße 15, 21073 Hamburg, Germany*

[2]*University of Vienna, Department of Physical Chemistry, Währinger Straße 42, 1090 Vienna, Austria*

[3]*Materials Design s.a.r.l., 18, rue de Saisset, 92120 Montrouge, France*

(Received 30 March 2012; revised manuscript received 19 June 2012; published 13 July 2012)

We discuss the structural details and the ordering of hydrogen in LaH_x for $2 \leqslant x \leqslant 3$. To this end, we combine first-principles calculations with the cluster-expansion method. This approach allows us to follow the H occupation of the interstitial sites within the face-centered cubic matrix of La atoms. We find that LaH_x clearly favors the fluorite structure at $x = 2$ and adds excess H atoms at the octahedral interstitial sites. The ground-state behavior of the system is discussed and is found in agreement with experimentally observed structures at compositions $LaH_{2.25}$ and $LaH_{2.50}$; an additional ground state at composition $LaH_{2.71}$ is predicted. The cluster expansion also permits an extensive scan of LaH_x structures with two octahedral vacancies per unit cell. For energetically favorable configurations, this scan yields a vacancy percolation threshold at $LaH_{2.75}$ that possibly drives the concentration-dependent metal-insulator transition: The band gap calculated for isolated vacancy pairs disappears for percolating vacancy chains. This transition from metallic to insulating state is also experimentally observed near to the composition $LaH_{2.8}$ and gives rise to the "switchable mirror" phenomenon.

DOI: 10.1103/PhysRevB.86.014107 PACS number(s): 71.15.Mb, 71.15.Nc, 61.72.Qq, 71.20.Eh

I. INTRODUCTION

There are still many empty patches on the phase diagram of the binary system La-H; e.g., the precise phase boundaries, structural details of the metal-rich and the H-rich phases, and the mechanisms of ordering on the H sublattice are not or only partially known. An estimated phase diagram of the La-H system for the whole accessible concentration range between the elemental metal and LaH_3, which was assessed from the available experimental data, can be found in Ref. 1.

Elemental La exists in three different modifications: The structure of the pure metal is double-hexagonal close packed (dhcp) at temperatures below 583 K, body-centered cubic (bcc) at temperatures between 1138 K and the melting point at 1191 K, and cubic close packed (ccp) at temperatures in between; see Ref. 1 and the references therein. Lanthanum of all allotropic forms dissolves H to a certain amount. The solubility of H in dhcp La seems to be low; see Ref. 2 and the references therein. Lanthanum hydride, which extends over the concentration range between about two and three equivalents of H, is in equilibrium with the solid solutions.

The hydride is described as a basically ccp metallic substructure with interstitially bonded H atoms. The latter show a preference for the occupation of the tetrahedral interstitial sites; e.g., the stoichiometric dihydride has a fluorite-type structure with occupied tetrahedral and vacant octahedral interstitial sites. This structure is prototypical for the dihydrides of all rare-earth metals, except for the divalent elements Eu and Yb. In overstoichiometric rare-earth dihydrides the octahedral interstitial sites are partially occupied in addition. For a discussion of the properties of rare-earth dihydrides, see Refs. 3–5. That the occupation of the octahedral sites commences after the occupation of the tetrahedral interstitial sites is completed is a somewhat simplified picture. Actually, octahedrally coordinated H atoms are already observed for slightly understoichiometric dihydrides. This phenomenon is related to the purity of the metal.[3,4] In the context of the present study, no *a priori* assumptions concerning the site preference are made. Whereas the hydrides of La and the light lanthanides Ce and Pr can be continuously hydrogenated without fundamental changes of the metallic matrix until the trihydride is reached, the (overstoichiometric) dihydrides of Sc, Y, and the heavier lanthanides are in equilibrium with the (understoichiometric) trihydrides with a basically hexagonal close-packed metallic matrix.

With the trihydride LaH_3, which is commonly assumed to have a cubic structure of the $D0_3$ type (Strukturbericht designation), the H-rich boundary of the La-H system is reached. The optimization of the structure of the stoichiometric trihydride, however, led to an orthorhombically distorted structure with four formula units per unit cell and the lattice constants $a = 8.010$ Å, $b = 5.289$ Å, $c = 4.079$ Å; the structure is described on the basis of space group type *Pnma* (No. 62) with La atoms occupying Wyckoff position 4*c* ($x = 0.12974$, $z = 0.71477$), tetrahedrally coordinated H atoms at Wyckoff position 8*d* ($x = 0.11804$, $y = 0.00209$, $z = 0.20169$), and octahedrally coordinated H atoms at Wyckoff position 4*c* ($x = 0.36438$, $z = 0.15679$).[5,6] The orthorhombic distortion goes along with a lowering of the total energy by 21 meV per formula unit. We deploy the *Pnma* structure as reference for the H-rich side of the phase diagram.

Previously, LaH_x was found to undergo structural transformations in the composition region between $x = 2$ and $x = 3$ which are connected with tetragonal distortions of the arrangements of the La atoms,[7] displacements of the octahedrally coordinated H atoms along the ⟨111⟩ directions,[8,9] and the formation of tetragonal superstructures as a consequence of H ordering at $x = 2.25$ and $x = 2.50$.[10–12]

Like the hydrides of other rare-earth metals, LaH_x exhibits a concentration-dependent metal-insulator transition between $x = 2$ and $x = 3$,[3,4,13] which is connected to the so-called "switchable-mirror" phenomenon:[14] Thin films of La and

other rare-earth metals can be reversibly switched between the metallic and the insulating state by changing the H content of the sample. The transition is attended by an abrupt change of the optical properties. This effect can be used as transducer principle in sensor technology; see Ref. 15 and the references therein.

II. COMPUTATIONAL DETAILS

A. Structure optimizations, total-energy and electronic-structure calculations

The optimizations and the calculation of the total energies of several hundred model structures for LaH_x with a cubic close-packed arrangement of the La atoms probing the whole accessible concentration range between $x = 0$ and $x = 3$ as well as the computation of electronic densities of states (DOS) for selected structures were carried out by means of the Vienna *Ab initio* Simulation Package (VASP).[16–19] The Kohn-Sham equations of density-functional theory (DFT)[20,21] with periodic boundary conditions were solved within plane-wave basis sets with electron-ion interactions described by potentials constructed according to the projector-augmented-wave method[22,23] with a [Kr]$4d^{10}$ La core, i.e., considering also the La $4f$ states as valence states. A cutoff energy of 500 eV was chosen for the plane-wave basis sets. Exchange and correlation were treated within the generalized-gradient approximation.[24] Scalar relativistic effects were included. Spin-polarization was excluded. For reciprocal-space sampling, Γ-centered Monkhorst-Pack $\boldsymbol{k}$ meshes[25] were used that correspond to a distance between nearest-neighbor $\boldsymbol{k}$ points of about 0.2 $Å^{-1}$ or below. Such $\boldsymbol{k}$ meshes had turned out to be a good compromise between the numerical effort involved and the accuracy of the calculated energies of formation (see Sec. II C), if the latter are obtained from total energies of structures based on the same unit cell. Reciprocal-space integration was performed with the first-order Methfessel-Paxton method[26] with a broadening parameter of 0.2 eV. Structural parameters (lattice parameters and ionic positions) were optimized by minimizing the atomic forces and the stress tensor with respect to all crystallographic degrees of freedom applying the conjugate gradient technique implemented in VASP.

B. Cluster expansion

While DFT calculations provide accurate information about the energies of selected structures, they cannot supply a comprehensive view of all possible fully relaxed atomic structures. In order to obtain such comprehensive, fast, and reliable information for La-H beyond the DFT results, we mapped their multibody, fully relaxed energetics onto a cluster expansion[27–30] (CE) by using the UNCLE code.[30]

The parent lattice for the expansion was an fcc base lattice with a four-site basis defining four sublattices: The first sublattice constitutes a primitive fcc lattice; the two tetrahedral and the one octahedral interstitial sites per unit cell make up the other three sublattices. The La atoms completely occupy the first sublattice, while the H atoms can occupy the interstitial sites. Those interstitial sites that are not occupied by H are "occupied" by a vacancy instead. For a CE, the configuration space is thus a ternary space, with possible La, H, and vacancy occupations. But since the fcc matrix of the La atoms is fixed, neither the fcc sublattice containing the matrix atoms nor the La occupation itself has to be included in the CE. This leaves us with a binary problem: We consider a structure σ as a binary "compound" of interstitial sites occupied by H (■) and vacant interstitial sites (□); i.e., LaH_x is treated as $■_x□_{3-x}$. The CE will describe the two possible occupations ■ and □ as mathematical spins ±1.

On this lattice, a CE for the formation energy $E_f(\sigma)$ (defined and explained in detail in Sec. II C) of an arbitrary atomic structure σ was constructed:

$$E_f(\sigma) = \sum_{C \in \boldsymbol{C}} J_C \Pi_C(\sigma). \tag{1}$$

The form of Eq. (1) is of a generalized Ising model. Here, a cluster C simply represents the interaction between several lattice sites that are part of the cluster and are occupied by spins ±1. The free parameters J_C (the so-called effective cluster interactions) account for the interaction strength of a certain cluster C, and the correlations $\Pi_C(\sigma)$ incorporate the structure dependence of $E_f(\sigma)$ by a product of the occupational spins of the cluster C on the lattice.[31] In the concentration region between the dihydride LaH_2 and the trihydride LaH_3, the values J_C were adjusted by least-squares fitting so that the CE sum Eq. (1) reproduces the energetics of ≈250 DFT input structures. To this end, the genetic algorithm[32] of UNCLE[30] selected a set $\boldsymbol{C}$ of 27 clusters $C \in \boldsymbol{C}$, which describe the energetics in an optimal way. Apart from the empty cluster, 2 on-site, and 10 pair-interaction clusters, the set $\boldsymbol{C}$ also contains 14 many-body clusters that represent interactions between more than two sites. The error of the cluster selection was controlled by a (leave-many-out) cross-validation scheme and yielded a cross-validation score $S_{CV} = 3.51$ meV/La. We note that the CE, Eq. (1), with the parameters described in this paragraph is converged for structures with up to eight La atoms in an arbitrary supercell—i.e., the CE does not predict any energetically favorable structures that are not yet included as an input structure.

C. A binary formation energy for the cluster expansion

According to the previous section, a LaH_x structure σ can be viewed as a compound $LaH_x \mathrel{\widehat{=}} ■_x□_{3-x}$. Therefore, for a structure σ with mass formula LaH_x, we define that the *ab initio* formation energy $E_f(\sigma)$ is measured with respect to cubic close-packed elemental La and LaH_3 with *Pnma* symmetry. This is the energy corresponding to the reaction

$$\frac{x}{3}\,LaH_3 + \left(1 - \frac{x}{3}\right) La \longrightarrow LaH_x,$$

which is—from a chemical point of view—not a formation reaction in the usual sense. Nevertheless we follow the common practice and use the term "formation energy" henceforth, also for the ordinate of the CE-based ground-state diagram of the La-H system. The relevant reference points are not the pure chemical elements La and H_2 but the completely vacant ($x = 0$) and the completely occupied ($x = 3$) interstitial sublattice lattice of cubic close-packed La. If we identify the energy of one interstitial site of the completely occupied and the completely vacant interstitial lattice with $E(■) = \frac{1}{3}E(LaH_3)$

and $E(\square) = \frac{1}{3}E(\mathrm{La})$, respectively, the formation energy (in the usual sense) of configuration $\blacksquare_x\square_{3-x}$ corresponding to structure σ is given by $E_\mathrm{f}(\sigma)$. We calculated $E_\mathrm{f}(\sigma)$ in two steps:

(1) The total energy of σ per La atom, $E(\sigma)$, measured with respect to the total energies of cubic close-packed elemental La and cubic LaH_3, denoted by $E(\mathrm{La})$ and $E(\mathrm{LaH}_3^*)$, both given per La atom,

$$E_\mathrm{f}^*(\sigma) = E(\sigma) - \frac{x}{3}E(\mathrm{LaH}_3^*) - \left(1 - \frac{x}{3}\right)E(\mathrm{La}). \quad (2)$$

The three involved structures σ, La, and cubic LaH_3 are described on the basis of the same unit cell.

(2) The energy per La atom corresponding to the relaxation of cubic LaH_3 [with energy $E(\mathrm{LaH}_3^*)$ per La atom] leading to LaH_3 with *Pnma* structure associated with the total energy per La atom $E(\mathrm{LaH}_3)$,[5,6]

$$E_\mathrm{r} = E(\mathrm{LaH}_3) - E(\mathrm{LaH}_3^*) = 21\ \mathrm{meV}. \quad (3)$$

The formation energy of structure σ per La atom, $E_\mathrm{f}(\sigma)$, is now calculated as

$$E_\mathrm{f}(\sigma) = E_\mathrm{f}^*(\sigma) - \frac{x}{3}E_\mathrm{r}. \quad (4)$$

III. RESULTS AND DISCUSSION

The combination of DFT and CE provides a means to conduct a comprehensive survey of all possible structures σ up to a certain supercell size. It reveals their structural details, their relative energy, and their ordering at $T = 0$ K. For the La-H system, fundamental changes in the configurational ordering of H at octahedral interstitial sites take place in the region between the dihydride and the trihydride—changes that according to our theory eventually drive the concentration-dependent transition of LaH_x from the metallic to the insulating state.

The following Sec. III A will discuss the filling principle of the octahedral interstitial sites, the ground states of the system, and it will compare those results with experiment. The ordering of the interstitially bonded H atoms is left to Sec. III B, which will also discuss the influence on the metal-insulator transition near $LaH_{2.8}$. For those configurational studies at $T = 0$ K, we did not account for zero-point vibrations, which will also be justified in due course in Sec. III A.

A. Filling the octahedral interstitial sites

A CE scan for LaH_x over all structures with up to eight La atoms per unit cell, $N_\mathrm{La} \leqslant 8$, determines the fluorite structure as the most stable structure at $x = 2$; see Fig. 1, where the fluorite structure is highlighted. This finding corresponds to known experimental results.[3,4] As a matter of fact, the fluorite structure is much more stable than any other configuration at $x = 2$: There is a huge energy gap to the first excited state. The fluorite structure is also a ground state of the system. For our reasoning in the concentration range $2 \leqslant x \leqslant 3$, it constitutes the ground state with the lowest hydrogen concentration.

When we speak of ground states in that concentration range, see Fig. 1, it is also important to briefly address the energetics at lower concentrations (not shown in Fig. 1). For $x \leqslant 2$, there

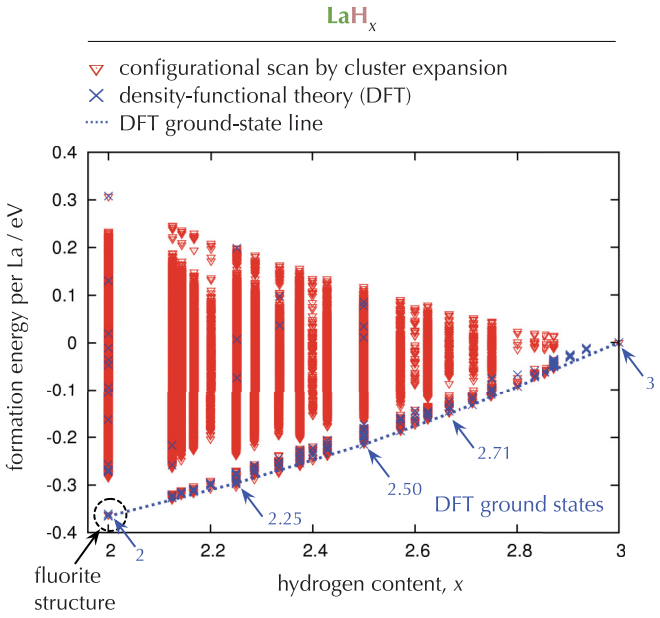

FIG. 1. (Color online) This ground-state diagram combines approximately 250 DFT energies with 969 770 energies from a CE scan with up to eight La atoms for $2 \leqslant x \leqslant 3$. The ground-state line is determined by the DFT energies. Its five vertices, the ground states, are marked by blue arrows. (For our definition of "formation energy" see Sec. II A.)

could in principle be a much deeper ground state that might downgrade the fluorite structure to a non-ground-state status. In order to eliminate this possibility, DFT calculations for $x < 2$ were combined with a preliminary CE in order to check for such ground states. The fluorite structure at $x = 2$ turned out to be indeed the configuration with the lowest energy of formation in the whole concentration range $0 \leqslant x \leqslant 3$. Therefore, it is not masked by any other ground state with $x < 2$, and the fluorite structure is a ground state.

When the hydrogen concentration exceeds $x = 2$, the system has to incorporate additional H atoms on free interstitial sites. The form of the ground-state diagram, Fig. 1, already suggests slight ordering tendencies of the interstitial-sites occupation: The system exhibits three more ground states before the trihydride is reached, which are marked by blue arrows and their concentration in Fig. 1. Nevertheless it should be noted that none of these three ground states for $2 < x < 3$ is as pronounced as the LaH_2 ground state. The other non-ground-state structures that are very close to the ground-state line simply constitute defect structures with a configuration that changed only slightly with respect to the ground states. The subsequent paragraphs will examine the ground states themselves and the general filling of the interstitial sites.

Following the natural intuition for the filling of the interstitial sites for $x > 2$, we look at $x = 2$: In the fluorite structure all tetrahedral interstitial sites are filled with H atoms, while all octahedral sites remain unoccupied. This structure proposes that as soon as more hydrogen is taken in by the La matrix, the additional H atoms reside at octahedral interstitial sites, while all the tetrahedral interstitial sites, which have already been occupied in the fluorite structure, remain occupied. Were the ground-state line between LaH_2 and LaH_3

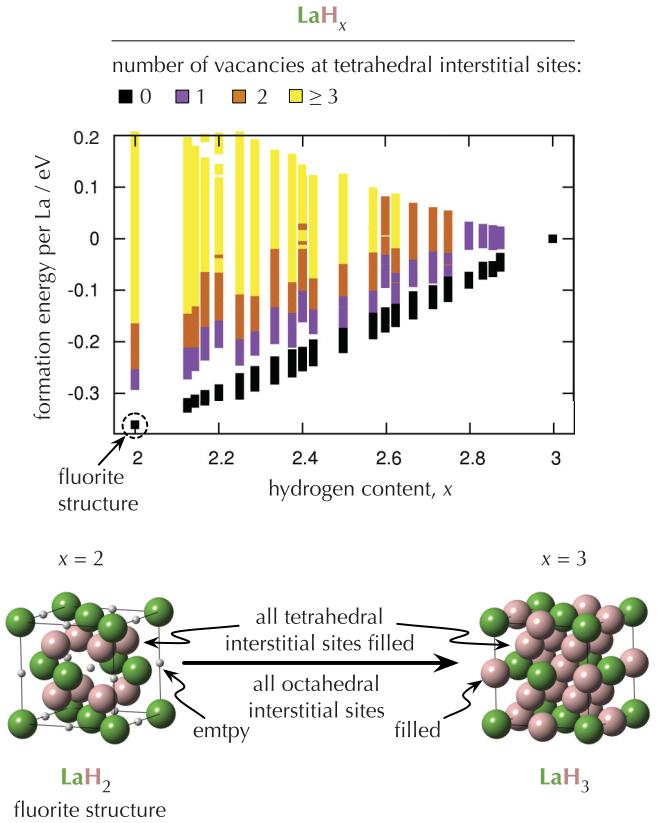

FIG. 2. (Color online) The CE energetics of Fig. 1 is overlaid by a color code that displays the number of unoccupied tetrahedral interstitial sites.

a straight line with no vertices in between, our proposition would certainly hold because then all ground-state structures in between—i.e., the structures on the ground-state line—would be simple mixtures of the ground-state structures of LaH_2 and LaH_3, which are characterized by a completely empty and a completely filled octahedral sublattice, respectively. Owing to the presence of three additional ordering ground states, however, the straightforward picture of simply filling the octahedral sites might as well fail. But the CE scans over all possible configurations and additionally provides structural information—for instance, information about which interstitial sites are occupied by H atoms.

Figure 2 confirms our simplistic considerations: It shows that at $T = 0$ K, all structures near the ground-state line—within an energetic perimeter of roughly 10 meV/La—have all their tetrahedral sites occupied by H and are therefore based on the fluorite structure. The "excess" H atoms—i.e., beyond two per La atom—occupy the octahedral positions. Only excited states, which are accessible by temperature effects, have tetrahedral vacancies and are thus not based on the fluorite structure. In Fig. 2, the energy differences per La atom between structures with one and structures without any tetrahedral vacancies depend on the unit-cell size of the respective structure. The lowest structure at each concentration (no tetrahedral sites vacant) and the first structure with one vacant tetrahedral site are separated by an energy difference (not shown) on the order of 500 meV *per unit cell* (in Figs. 1 and 2, the energy is given *per La atom*). This large energy

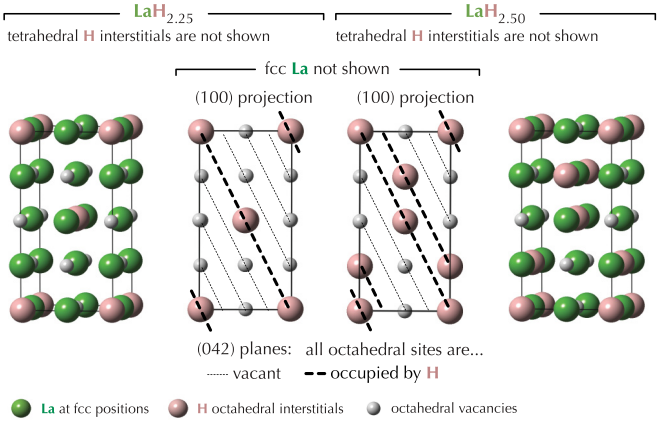

FIG. 3. (Color online) The ground-state structures at $LaH_{2.25}$ (left) and $LaH_{2.50}$ (right), found by density functional theory (DFT) as a result of the cluster expansion (CE) and confirmed by experiments (Refs. 10 and 11). The space groups are $I4/mmm$ and $I4_1/amd$, respectively. Both structures can be described as $1 \times 1 \times 2$ body-centered supercells of the conventional cubic unit cell. All tetrahedral sites are occupied and are not shown. For $LaH_{2.25}$, the octahedral occupation can be viewed as a $D0_{22}$ structure, and for $LaH_{2.50}$, the octahedral occupation can be associated with a 40 structure.

difference also vindicates our omission of zero-point energies, in particular with respect to the vibrational results about La-H presented in Ref. 2, and with respect to hydrogen studies at surfaces.[33] Although vibrational contributions may change the energies, they will not change the basic energetic hierarchy of the structures at $T = 0$ K.

Naturally, the ground states marked in Fig. 1 mirror this behavior: The occupation of the interstitial sites builds on the fluorite structure, and all tetrahedral interstitial sites are filled with H. From an experimental point of view, the ground state at $x = 2$ is well established.[3,4] Further experimental data of the crystal structures at $x = 2.25$ and $x = 2.50$ are available through neutron-powder-diffraction measurements of deuterium solved in a La matrix,[10,11] which can be set side by side with La-H. Accordingly, the discussion about the ground-state structures found by the CE will focus on the two structures at $x = 2.25$ and $x = 2.50$, their configurational details within the configuration space, their ordering of the octahedral hydrogens, and their geometric parameters determined by a full relaxation of the configurations by DFT; and both structures will be compared with the experiments by Udovic *et al.*[10,11] in the following. Figure 3 shows a real-space representation of the two ground-state structures at $x = 2.25$ and $x = 2.50$, which are presented in the next paragraphs; the ground-state structure at $x = 2.71$ will be briefly referred to in Sec. III B, but we already note here that its smallest possible unit cell has mass formula La_7H_{19} with two hydrogen vacancies situated on adjacent octahedral interstitial sites—a structural detail that will be essential in the general discussion of Sec. III B. For now, however, we focus on $LaH_{2.25}$ and $LaH_{2.50}$.

The ground state at $LaH_{2.25}$ is displayed on the left side of Fig. 3. Its smallest possible unit cell has mass formula La_4H_9, but it can also be viewed as a tetragonal body-centered $1 \times 1 \times 2$ supercell of the conventional cubic unit cell, in which case eight La atoms are present in the tetragonal unit cell. The

TABLE I. The table lists the geometric parameters of the ground-state structure $LaH_{2.25}$, space group $I4/mmm$, determined by our first-principles results (DFT) and compares them with the experimental values by Udovic *et al.* (Ref. 10), who investigated $LaD_{2.25}$ at $T = 15$ K. The coordinates for the La atoms at Wyckoff position 4*e* and of the tetrahedral H (D) atoms at Wyckoff position 16*n* are fractional coordinates. Values "0" express exact values (due to symmetry).

$LaH_{2.25}$		DFT	Experiment
a/Å		5.6082	5.6174(1)
c/Å		11.2879	11.3054(3)
La (4*e*)	x	0	0
	y	0	0
	z	0.2454	0.2459(2)
H (16*n*)	x	0.2587	0.2593(2)
	y	0.2587	0.2593(2)
	z	0.1267	0.1267(2)

TABLE II. The table lists the geometric parameters of the ground-state structure $LaH_{2.50}$, space group $I4/mmm$, as determined by our first-principles results (DFT) and compares them with the experimental values by Udovic *et al.* (Ref. 11), who investigated $LaD_{2.50}$ at $T = 10$ K. The coordinates for the La atoms at Wyckoff position 8*e* and of the tetrahedral H (D) atoms at Wyckoff position 16*f* are fractional coordinates. Values "0" and fractions express exact values (due to symmetry).

$LaH_{2.50}$		DFT	Experiment
a/Å		5.56884	5.59234(9)
c/Å		11.3086	11.2907(2)
La (8*e*)	x	0	0
	y	0	0
	z	0.7543	0.7540(1)
H (16*f*)	x	0.2690	0.2682(3)
	y	1/4	1/4
	z	1/8	1/8

symmetry of this cell is given by the space group $I4/mmm$ (No. 139). As expected, all tetrahedral interstitial sites of the fcc La matrix are occupied by H atoms (those interstitial sites are not shown in Fig. 3). The octahedral interstitial sites, on the other hand, are orderly occupied by H and H vacancies (■ and □, respectively, in the notation of Sec. II C) in such a way that the occupation of the octahedral interstitial sites forms a structure $■_1□_3$ analogous to $D0_{22}$ (Strukturbericht). Accordingly, every third (042) plane through this structure is completely filled with occupied octahedral sites, while all other (042) planes have only empty octahedral sites; see Fig. 3. These configurational details of the ground-state structure at $LaH_{2.25}$ correspond perfectly with the structure $LaD_{2.25}$ found by the experiment Ref. 10. Moreover, the geometric relaxations determined by the DFT calculation are in excellent agreement with the experimental data; see Table I.

The right side of Fig. 3 illustrates the ground-state structure at $LaH_{2.50}$. Its smallest possible unit cell has mass formula La_4H_{10} with two H vacancies on adjacent octahedral interstitial sites, a key detail for the general discussion in Sec. III B. The $LaH_{2.50}$ structure can be viewed as a $1 \times 1 \times 2$ tetragonal body-centered supercell of the conventional cubic unit cell, and its space group is $I4_1/amd$ (No. 141). Compared with the $LaH_{2.25}$ structure of the last paragraph, more octahedral interstitial sites are now filled with H atoms, and two (042) planes devoid of octahedral hydrogens alternate with two (042) planes completely filled with octahedral hydrogens. Thus, the octahedral ordering can be described as an artificial Strukturbericht 40 structure $■_2□_2$. Once more, the configuration described here agrees with the experimental structure $LaD_{2.50}$ of Ref. 11. Additionally, the DFT structure optimization and the experiment by Udovic *et al.*[11] harmonize perfectly in the geometric parameters that describe the structural relaxations; see Table II.

The octahedral interstitial sites dominate the structural changes between LaH_2 and LaH_3. Their filling up and their ordering in the ground-state structures—both presented in this section—clearly corroborate this view. The next section will take a closer look at the ordering of octahedral vacancies in this concentration range.

B. Percolating vacancies and the metal-insulator transition

Except for the trihydride LaH_3, none of the ground states marked in Fig. 1 exhibits a band gap. The lack of a band gap in fluorite-type LaH_2 and the $D0_{22}$-like structure of $LaH_{2.25}$ (see previous section) can easily be inferred from their odd number of valence electrons per unit cell. Since every H and La atom contributes with 1 and 3 valence electrons, the ground states of LaH_2 and $LaH_{2.25}$ have 5 and 21 valence electrons per primitive unit cell (viz., unit cells corresponding to formulas La_1H_2 and La_4H_9) and thus cannot exhibit a band gap. For the ground-state structures with an even number of valence electrons, the existence or nonexistence of a band gap was checked by DFT calculations of the electronic DOS (not shown). They confirmed that the ground states at $LaH_{2.50}$ and $LaH_{2.71}$ are metallic, which is the expected result because experiments find the metal-insulator transitions not until around $LaH_{2.8}$.[3,13] For the LaH_3 structure, a band gap appears and the solid is insulating[6]—also in accordance with experimental results.

So, somewhere between $x = 2.71$ and $x = 3$ it happens: the transition from metallic structures without a band gap to insulating structures with a band gap. The appearance of the transition at intermediate values of x follows directly from the presence of the ground states at $x = 2.71$ and $x = 3$. But what is the critical hydrogen concentration? And even more interesting: What configurational process prompts this transition? What is the main difference between the structures $LaH_{2.71}$ and structures close to LaH_3? Even if all structures on the ground-state line between $x = 2.71$ and $x = 3$ are mixtures of the ground states $LaH_{2.71}$ and LaH_3, the band gap of those structures cannot simply be extrapolated as something like a "mixture" of those of $LaH_{2.71}$ and LaH_3. The question about the critical H concentration is answered by experiments: The transition occurs approximately at $x = 2.8$.[3,13] Without answer, however, remain the questions about the configurational process prompting the transition and the main difference between metallic and insulating hydrides. We approach those questions in a two-step process: In the next paragraph, we will use the energetics of the CE to find the configurational change between $LaH_{2.71}$ and LaH_3; afterwards, DFT calculations for the electronic DOS will lend support to

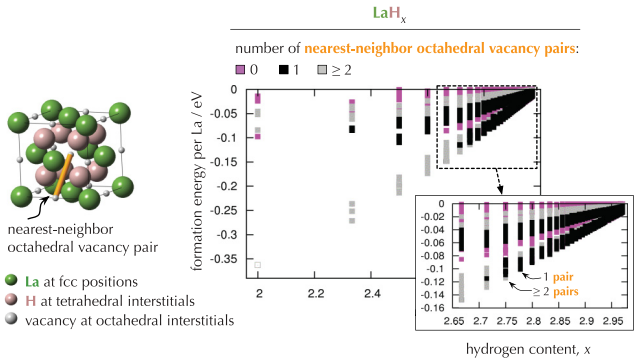

FIG. 4. (Color online) The figure shows the energetics of a CE scan over all configurations with exactly two H vacancies, $La_{N_{La}}H_{3N_{La}-2}$, for selected $N_{La} \leqslant 68$. The color code reveals the formation of vacancy chains: It indicates the number of nearest-neighbor octahedral vacancy-vacancy "bonds" in each structure; see the illustration on the left. At a hydrogen concentration $x \geqslant 2.78$, the two H vacancies in each structure form exactly one nearest-neighbor pair, and those pairs are isolated from each other. When the H concentration decreases, $x \leqslant 2.75$, more nearest-neighbor vacancy pairs form (gray boxes). Since each structure's unit cell comprises precisely two vacancies, more nearest-neighbor pairs are tantamount to the formation of vacancy chains, created by the translational symmetry of the cells.

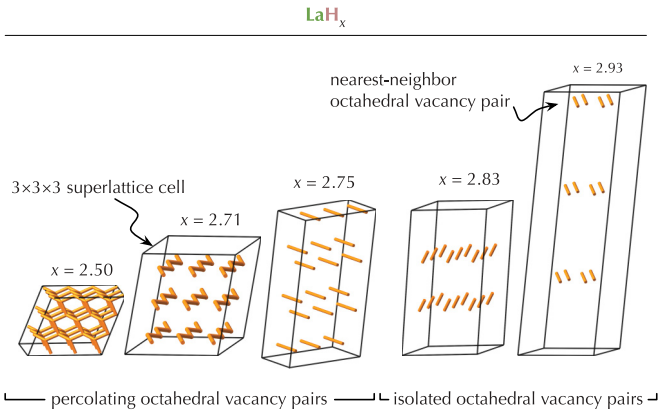

FIG. 5. (Color online) The octahedral vacancy bonds discussed in Fig. 4 are shown for five selected structures, which are the energetically most favorable structures at the given concentrations, determined by the CE scan of Fig. 4. All structures are either ground states ($x = 2.50$, $x = 2.71$) or deviate only slightly (< 1 meV/La) from the DFT ground-state line of Fig. 1. The chosen concentrations are above (left) or below (right) the percolation threshold near $x = x_c = 2.75$. For clarity, no La or H atoms are shown, and all the structures are depicted within a $3 \times 3 \times 3$ supercell of the unit cell with the least volume. In this way, the bonds become more clearly visible. Owing to the periodicity, the bonds within each structure are all alike. Note that bonds crossing the boundaries of the supercell are not shown.

our assertion that the configurational change found with the CE indeed drives a metal-insulator transition. The first step is taken by the structural information that the CE provides: information about pairs of octahedral H vacancies.

In the dilute-vacancy limit near the trihydride, close nearest-neighbor pairs of octahedral vacancies are favored over two separated vacancies, a fact already known from previous DFT studies[6] and also reflected in the ground-state structures $LaH_{2.50}$ and $LaH_{2.71}$. The configurational scan of Fig. 4 expands the DFT results to all possible configurations with exactly two vacancies per unit cell for $N_{La} \leqslant 68$ La atoms. Such a scan became only possible with the latest algorithm by Hart *et al.* of Ref. 34. We emphasize that Fig. 4 is not simply a close-up of the energetics in Figs. 1 or 2. Instead, Fig. 4 shows the energetics of configurations with particular properties, namely, configurations with exactly two hydrogen vacancies per unit cell. The presence of exactly two hydrogen vacancies per unit cell is an important prerequisite for the following. The number of nearest-neighbor "bonds" connecting octahedral vacancies is color coded in Fig. 4, which proves that at high hydrogen concentrations the octahedral vacancies form isolated pairs: The energetically favorable structures exhibit exactly one nearest-neighbor vacancy-vacancy bond between octahedral sites, which is tantamount to one isolated pair of octahedral vacancies. Only when the H concentration decreases to approximately $x \approx 2.75$, more bonds between H vacancies become visible. But in our model setting of two vacancies per unit cell, more bonds are equivalent to chains of vacancies that percolate through the system: Two vacancies can at most form one single bond within the unit cell, and if two bonds or more develop, it must be due to the translational periodicity of the unit cell, when the one pair within the unit cell connects to the pair in the next repeating unit cell, hence generating a whole percolating chain of pairs.

Figure 4 establishes the critical percolation threshold of the system at $x = x_c = 2.75$, which corresponds to a unit cell La_8H_{22} with a critical octahedral-vacancy concentration of $\xi_c = 2/8 = 0.25$, because all but two of the eight octahedral sites in La_8H_{22} are occupied. The significance of ξ_c will be further discussed below. Figure 5 supplies "real-space" evidence for the reasoning above. Instead of counting the vacancy-vacancy bonds, it displays those bonds for five selected structures, which are the lowest-energy structures above and below the percolation threshold, as predicted by the CE (Fig. 4).

The structural change from percolating vacancy chains at concentrations $x < x_c$ to isolated vacancy pairs at $x > x_c$ seems to be responsible for the metal-insulator transition in La-H, and potentially in other systems like Y-H. According to Ref. 6, isolated octahedral vacancy pairs at concentrations close to the trihydride aggregate electronic charge from the surrounding La atoms. Our above findings suggest that this charge be trapped below the percolation threshold at high H concentrations, $x > x_c$, because the vacancy pairs are isolated, and so the structures are insulators. Above the threshold (at lower H concentrations, $x < x_c$), the percolating vacancy pairs set the electrons free, and the material LaH_x becomes metallic. The vacancy chains therefore serve as tubes through which the electrons can move to conduct electricity. Figure 6 corroborates these findings by juxtaposing several different alignments of octahedral vacancies in a cubic La_{32} cell with the corresponding electronic DOS. The vacancies can either form isolated pairs or chains of pairs that percolate through the system. For the isolated pairs, the DOS exhibits a band gap that is the more pronounced the farther away from each other

the vacancy pairs are. Thus, those structures are insulators. On the other hand, the chain structures yield a DOS without a band gap, and the structures are metallic.

The last few paragraphs illuminated the metal-insulator transition in La-H and explained it with the change from percolating vacancy chains to isolated vacancy pairs. Critical phenomena like percolation have been studied in details for years. In La-H, the percolation threshold at $x_c = 2.75$ corresponds to a critical octahedral-vacancy concentration of $\xi_c = 0.25$; see above. The picture of "octahedral-vacancy concentration" ξ reverses the picture of "hydrogen concentration," as LaH_3 has $\xi = 0$, and LaH_2 has $\xi = 1$. The isolated octahedral sublattice is an fcc lattice like the one of the La matrix, but only shifted by half a lattice constant along one edge of the conventional cubic unit cell. Provided one starts at LaH_3 ($\xi = 0$) and *randomly* inserts vacancies into the octahedral sublattice with probability p per fcc site, the question of percolating vacancies is the question of site percolation on an fcc lattice. There, the critical percolation threshold is known from Monte Carlo simulations to be $p_c = 0.1992365(10)$.[35] Clearly, $\xi_c > p_c$. So, percolating clusters are generated more easily by inserting octahedral vacancies at random than by forming orderly aligned chains like in La-H?

Had the system La-H the tendency and preference to form those percolating vacancy chains, then one would expect a percolation threshold ξ_c much smaller than p_c. Ordering of the pairs to long chains would soon enough force a percolation transition long before the limit p_c of the random distribution, $\xi_c < p_c$. Even at small vacancy concentrations, percolating chains can be constructed by ordering the vacancies "by hand" (Fig. 6). The system itself, however, will not accept this ordering: Compared with the isolated pairs, the chain arrangement is energetically unfavorable at high concentrations. And so unfavorable it also remains at lower hydrogen concentrations until, finally, at x_c (or ξ_c, respectively) the octahedral occupation is thinned out enough to give way to the vacancy chains.

The result that the vacancy-percolation threshold in La-H is larger than the threshold of a purely random distribution, $\xi_c > p_c$, simply illustrates the fact that the formation of isolated vacancy-vacancy pairs is more favorable in La-H than the formation of chains. Even if the chains are not especially unsuited for obtaining low energies, they are not able to lower the percolation threshold below p_c; on the contrary, it turns out that the percolation threshold is even shifted to slightly higher octahedral-vacancy concentrations. For the system it is not irrelevant how the octahedral vacancies are ordered, whether they are randomly distributed or aligned in long-range clusters or in very short-range isolated pairs. The tendency is distinctly towards intimate pairs. And those pairs want to form as soon as possible when the hydrogen concentration is increased, and they want to stick together as long as possible when the hydrogen concentration is lowered. By clinging together, the octahedral vacancies push back the influence of the fluorite structure and lower the critical concentration x_c. Hence, the metal-insulator transition of La-H and its critical concentration reveal a configurational conflict: the conflict between the isolated pairs, which are clearly favored at high concentrations, and the percolating vacancy chains, which occur below $x_c = 2.75$.

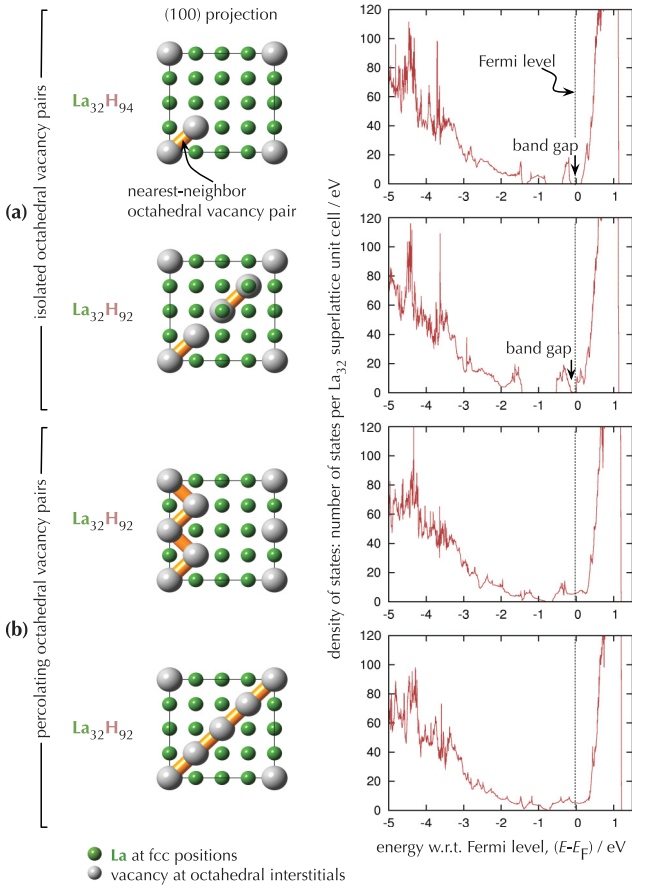

FIG. 6. (Color online) The figure shows the electronic DOS for four selected La_{32} configurations inside a $2 \times 2 \times 2$ superlattice of the conventional cubic unit cell. The structures differ in the way the octahedral vacancy pairs are aligned. For clarity, no H atoms are shown in the given (100) projections, and the octahedral vacancies are depicted as large gray spheres with orange nearest-neighbor bonds (cf. Figs. 4 and 5). In the plot of the DOS, the Fermi level is indicated by a dashed line. (a) In the two topmost structures, the vacancy pairs are isolated. The farther away from each other the pairs are, the more pronounced is the band gap at the Fermi level. The band gap in the $La_{32}H_{92}$ structure, where the vacancy pairs are relatively close together, hardly develops at all, and a small fraction (roughly 1%) of one electronic state is present up to the Fermi level. (b) As soon as the vacancy pairs percolate through the system—e.g., by formation of one-dimensional structures like a zigzag line or a linear arrangement—the band gap vanishes.

IV. CONCLUSIONS

The present first-principles work sheds some light on the structural details and the ordering of LaH_x structures in the concentration region $2 \leqslant x \leqslant 3$, and it furthermore presents an explanation for the metal-insulator transition. To this end, DFT calculations joined forces with the cluster expansion (CE).

On the one hand, starting with the fluorite structure at $x = 2$, we showed that additional H atoms are incorporated at octahedral interstitial sites. The ground states that we found at $LaH_{2.25}$ and $LaH_{2.50}$ agree excellently with experiments. Both our theoretical results and the experimental data exhibit an ordering of the hydrogen occupation at octahedral interstitial

sites analogous to $D0_{22}$ and 40; the geometric parameters correspond perfectly.

On the other hand, at high hydrogen concentrations near the trihydride, the vacancies at octahedral sites form isolated pairs. As had already been shown in Ref. 6, those isolated pairs accumulate charge from the surrounding La atoms. Decreasing the H concentration, our CE scan demonstrated that it is not before $x = 2.75$ that the isolated vacancy pairs give way to percolating vacancy chains. We proposed that those percolating vacancy chains release the once accumulated charge, thus close the band gap observed for isolated vacancy pairs, and explain the metal-insulator transition in La-H and probably similar systems. This view was corroborated by DOS calculations for several structures, which yield a band gap for isolated vacancy pairs and a metallic DOS for percolating vacancy chains.

By exploiting the combination of DFT and CE, our work indicates how important it is to have sound knowledge of both the electronic structure of selected atomic configurations and the overall energetics of the system.

ACKNOWLEDGMENTS

The authors T.C.K. and R.P. gratefully acknowledge the support of the Austrian Science Fund FWF for Project No. F4110 "ViCoM," and the authors G.S. and P.H. for FWF Project No. P19205-N19. Parts of the calculations have been performed on the Vienna Scientific Cluster.

*tobias.kerscher@tuhh.de

[1] D. Khatamian and F. D. Manchester, Bull. Alloy Phase Diagrams **11**, 90 (1990).
[2] G. Schöllhammer, P. Herzig, W. Wolf, P. Vajda, and K. Yvon, Phys. Rev. B **84**, 094122 (2011).
[3] P. Vajda, in *Handbook on the Physics and Chemistry of Rare Earths*, edited by K. A. Gschneidner Jr., and L. Eyring (Elsevier, Amsterdam, 1995), Vol. 20, Chap. 137.
[4] P. Vajda, in *Properties of Fluorite Structure Materials*, edited by P. Vajda and J. M. Costantini (Nova Science Publishers, New York, in press).
[5] G. Schöllhammer, F. Karsai, and P. Herzig, in *Properties of Fluorite Structure Materials*, edited by P. Vajda and J. M. Costantini (Nova Science Publishers, New York, in press).
[6] G. Schöllhammer, W. Wolf, P. Herzig, K. Yvon, and P. Vajda, J. Alloys Compd. **480**, 111 (2009).
[7] P. Klavins, R. N. Shelton, R. G. Barnes, and B. J. Beaudry, Phys. Rev. B **29**, 5349 (1984).
[8] P. Fischer, W. Hälg, L. Schlapbach, and K. Yvon, J. Less-Common Met. **60**, 1 (1978).
[9] G. Renaudin, K. Yvon, W. Wolf, and P. Herzig, J. Alloys Compd. **404–406**, 55 (2005).
[10] T. J. Udovic, Q. Huang, J. J. Rush, J. Schefer, and I. S. Anderson, Phys. Rev. B **51**, 12116 (1995).
[11] T. J. Udovic, Q. Huang, and J. J. Rush, J. Solid State Chem. **122**, 151 (1996).
[12] T. J. Udovic, Q. Huang, C. Karmonik, and J. J. Rush, J. Alloys Compd. **293–295**, 113 (1999).
[13] R. G. Barnes, C. T. Chang, G. Majer, and U. Kaess, J. Alloys Compd. **356–357**, 137 (2003).
[14] J. N. Huiberts, R. Griessen, J. H. Rector, R. J. Wijngaarden, J. P. Dekker, D. G. de Groot, and N. J. Koeman, Nature (London) **380**, 231 (1996).
[15] A. Remhof and A. Borgschulte, Eur. J. Chem. Phys. Phys. Chem. **9**, 2440 (2008).
[16] G. Kresse and J. Hafner, Phys. Rev. B **47**, 558 (1993).
[17] G. Kresse and J. Hafner, Phys. Rev. B **49**, 14251 (1994).
[18] G. Kresse and J. Furthmüller, Phys. Rev. B **54**, 11169 (1996).
[19] G. Kresse and J. Furthmüller, Comput. Mater. Sci **6**, 15 (1996).
[20] P. Hohenberg and W. Kohn, Phys. Rev. **136**, B864 (1964).
[21] W. Kohn and L. J. Sham, Phys. Rev. **140**, A1133 (1965).
[22] P. E. Blöchl, Phys. Rev. B **50**, 17953 (1994).
[23] G. Kresse and D. Joubert, Phys. Rev. B **59**, 1758 (1999).
[24] J. P. Perdew, J. A. Chevary, S. H. Vosko, K. A. Jackson, M. R. Pederson, D. J. Singh, and C. Fiolhais, Phys. Rev. B **46**, 6671 (1992).
[25] H. J. Monkhorst and J. D. Pack, Phys. Rev. B **13**, 5188 (1976).
[26] M. Methfessel and A. T. Paxton, Phys. Rev. B **40**, 3616 (1989).
[27] J. M. Sanchez, F. Ducastelle, and D. Gratias, Physica A **128**, 334 (1984).
[28] J. W. D. Connolly and A. R. Williams, Phys. Rev. B **27**, 5169 (1983).
[29] G. D. Garbulsky and G. Ceder, Phys. Rev. B **51**, 67 (1995).
[30] D. Lerch, O. Wieckhorst, G. L. W. Hart, R. W. Forcade, and S. Müller, Modelling Simul. Mater. Sci. Eng. **17**, 055003 (2009).
[31] For a more thorough view on some practical aspects of CEs see Refs. 30 and 36.
[32] G. L. W. Hart, V. Blum, M. J. Walorski, and A. Zunger, Nat. Mater. **4**, 391 (2005).
[33] D. Lerch, O. Wieckhorst, L. Hammer, K. Heinz, and S. Müller, Phys. Rev. B **78**, 121405(R) (2008).
[34] G. L. W. Hart, L. J. Nelson, and R. W. Forcade, Comp. Mat. Sci. **59**, 101 (2012).
[35] C. D. Lorenz and R. M. Ziff, J. Phys. A: Math. Gen. **31**, 8147 (1998).
[36] S. Müller, J. Phys.: Condens. Matter **15**, R1429 (2003).